

Corrosion- and wear-resistant properties of Ni–Al₂O₃ composite coatings containing various forms of alumina

S. T. Aruna · V. Ezhil Selvi · V. K. William Grips ·
K. S. Rajam

Received: 22 April 2010 / Accepted: 4 February 2011 / Published online: 20 February 2011
© Springer Science+Business Media B.V. 2011

Abstract This article describes the effect of the addition of different phases of alumina particles on the properties of electrodeposited Ni–Al₂O₃ composite coatings. The corrosion- and wear-resistant properties of Ni–Al₂O₃ composite coatings electrodeposited from a nickel sulfamate bath containing (i) alpha-alumina particles (Ni–Al₂O₃-1), (ii) gamma-alumina particles (Ni–Al₂O₃-2), and (iii) mixture of alpha, gamma, and delta alumina particles (Ni–Al₂O₃-3) have been studied. The potentiodynamic polarization and electrochemical impedance spectroscopy (EIS) studies showed superior corrosion resistance of Ni–Al₂O₃-2 composite coatings compared with other two coatings. The SEM images and EDAX spectra also corroborated well with the observed corrosion results. The pin-on-disk wear studies showed improved wear resistance of Ni–Al₂O₃-1 composite coating containing alpha alumina compared with other two coatings. The transfer of material from the pin onto the disk was evident from the optical microscopy images of the wear tracks and Raman spectra of the wear track. This study shows that the addition of pure gamma-alumina particles enhances the corrosion resistance, and that pure alpha-alumina particles enhance the wear resistance of Ni composite coatings to a greater extent.

Keywords Ni · Alumina · Corrosion · Wear · Microhardness

1 Introduction

Electrodeposited nickel composite coatings containing ceramic particles like Al₂O₃, TiO₂, ZrO₂, SiC, Si₃N₄, etc. are the most widely studied and reported in the literature. Alumina (Al₂O₃) is the most widely used ceramic because of its superior properties like good chemical stability, high microhardness, and wear resistance at high temperature and lower cost. There have been a large number of publications on electrodeposition of Ni–Al₂O₃ composite coatings by varying the deposition parameters [1–12]. The corrosion resistance of composite nickel electrodeposits with alumina embedded in the nickel matrix prepared in sulfate and chloride bath has been reported [13]. Improved corrosion resistance of electrochemically deposited Ni–Al₂O₃ from a Watts bath has also been reported [14]. Electrochemical impedance spectroscopy (EIS) and corrosion behavior of Ni–Al₂O₃ nanocomposite coatings have been reported by Ciubotariu et al. [15]. Szczygiel and Kolodziej [16] have studied the corrosion resistance of Ni–Al₂O₃ coatings in NaCl solution. Improved microhardness and wear resistance for Ni–Al₂O₃ and Ni–SiC composite coatings have been reported by Wang and Wei [17]. Feng et al. [18] have observed an improved wear resistance for nanostructured Ni/Al₂O₃ composite coatings deposited under the influence of an external high magnetic field (8T). Most of the reported literature have discussed the synthesis and properties of Ni–Al₂O₃ composite coatings containing mostly α -alumina particles. In a recent article, we have reported the preparation of Ni–Al₂O₃ composite coatings containing different crystallographic forms of alumina [19]. To the best of our knowledge, there are no reports on the comparative study on the corrosion- and wear-resistant properties of Ni–Al₂O₃ composite coatings containing different phases of alumina. It is interesting to investigate the effect

S. T. Aruna (✉) · V. Ezhil Selvi · V. K. William Grips ·
K. S. Rajam
Surface Engineering Division, Council of Scientific
and Industrial Research-National Aerospace Laboratories,
P.O. Box 1779, Bangalore 560 017, India
e-mail: aruna_reddy@nal.res.in

of different phases of alumina on the properties of Ni–alumina composite coatings. The aim of this study was to investigate the corrosion- and wear-resistant properties of electrodeposited Ni–Al₂O₃ composite coatings containing different forms of alumina.

2 Experimental

The Al₂O₃ particles prepared from (i) solution combustion process containing pure alpha alumina (crystallite size 40 nm), (ii) precipitation method containing pure gamma alumina (crystallite size 5 nm) and (iii) commercial alumina (Alcoa) powder with a crystallite size of 40 nm containing mixture of alpha, gamma, and delta crystalline phases were dispersed in a nickel sulfamate bath and stirred well overnight. Details regarding the preparation and characterization of alumina powders and Ni–alumina composite coatings have already been published [19]. The Ni–alumina composite coatings (i) Ni–Al₂O₃-1 (containing combustion synthesized alumina), (ii) Ni–Al₂O₃-2 (containing precipitation synthesized alumina), and (iii) Ni–Al₂O₃-3 (containing commercial alumina) were electrodeposited at 15.5 mA cm⁻² for 36 min at 600 rpm (magnetic stirring). The coating thickness of the samples for corrosion studies was maintained at 11 ± 1 µm on mild steel substrate. To study the effect of current density on particle incorporation, the plating was carried out on brass coupons, and the thickness was not controlled precisely.

The microhardness and particle distribution of the composite coatings electrodeposited at 15.5 mA cm⁻² at 600 rpm were measured at least on five different areas on the cross section of polished samples using a microhardness tester (Micromet 2103, Buehler, 50 gf load) and vertical metallurgical optical microscope.

Electrochemical studies on Ni–alumina-coated, circular-shaped mild steel samples were conducted using Autolab PGStat-30 (Potentiostat/galvanostat) system. The test was conducted in free air 3.5% NaCl solution (0.6 N). Platinum foil of 1 cm² area was used as the counter electrode, and Ag/AgCl (3 M KCl) was used as the reference electrode. Details of corrosion testing had already been reported [20].

The tribological performance of Ni–alumina composite coatings was investigated by conducting wear tests on a pin-on-disk tribometer (DUCOM, India) under ambient conditions of temperature and humidity (30 °C, 50% RH) at an applied load of 9.8 N. Wear experiments were undertaken for a minimum of three specimens on semi-circular brass pins of radius 6 mm coated with Ni–Al₂O₃. Brass pins were coated with Ni–Al₂O₃ coatings by electrodeposition at 15.5 mA cm⁻² for 3 h (~40 µm thickness). All the wear tests were conducted at a wear track radius of 30 mm and 200 rpm (slide speed of 0.628 m s⁻¹)

to get a constant sliding distance of 4525 m. Hardened EN 31 steel disk with a Vickers hardness of 750 HV was used as the counter part. More details regarding the wear studies have already been reported [21]. The wear coefficient was calculated using the Holm–Archard relationship [22, 23]. The Raman spectra of the wear tracks on the disks and pins were recorded using a DILOR-JOBIN-YVON-SPEX (Paris, France) integrated Raman Spectrometer (Model Labram).

3 Results and discussion

The microhardness of Ni–Al₂O₃ composite coatings electrodeposited at 15.5 mA cm⁻² at 600 rpm was found to be 483 ± 19, 390 ± 9, and 350 ± 12 KHN, respectively for Ni–Al₂O₃-1, Ni–Al₂O₃-2, and Ni–Al₂O₃-3. The higher microhardness of Ni–Al₂O₃-1 may be attributed to the relatively higher microhardness of α-alumina compared to γ-alumina particles. The grain size of nickel was 25, 16, and 11 nm respectively for Ni–Al₂O₃-1, Ni–Al₂O₃-2, and Ni–Al₂O₃-3. The cross-sectional optical microscope images of the composites are shown in Fig. 1. The alumina particles in Ni–Al₂O₃-1 are in the form of various irregular-shaped particles, and in the case of Ni–Al₂O₃-2, more number of spherical particles are observed with a very few irregular-shaped particles. Ni–Al₂O₃-3 exhibits more number of particles with less agglomeration. From the optical microscope images, it is clearly seen that the area fraction of particles in the Ni–Al₂O₃-3 coating was higher. The area fractions of particles in the nickel matrix were 7.5, 13, and 17% respectively for Ni–Al₂O₃-1, Ni–Al₂O₃-2, and Ni–Al₂O₃-3.

3.1 Corrosion resistance

The potentiodynamic polarization curves obtained for Ni and Ni–Al₂O₃ composite coatings are shown in Fig. 2. The corrosion potential, the corrosion current, and the polarization resistance obtained from the Tafel plots are listed in Table 1. When compared to the uncoated substrate, the corrosion potential of the coated samples shifted toward more positive side, indicating improved corrosion resistance of the coatings. Plain Ni showed corrosion potentials of -0.451 V and the corrosion current density of 0.6267 µA cm⁻². In the case of Ni–Al₂O₃, corrosion potentials ranging from -0.267 to -0.184 V. The corrosion current density is an important parameter used for evaluating the kinetics of the corrosion reaction. Corrosion protection is inversely proportional to the corrosion current density. The corrosion current density for the nanocomposite coatings varied from 0.0119 to 0.0839 µA cm⁻². The corrosion current density of the Ni–Al₂O₃-2 was

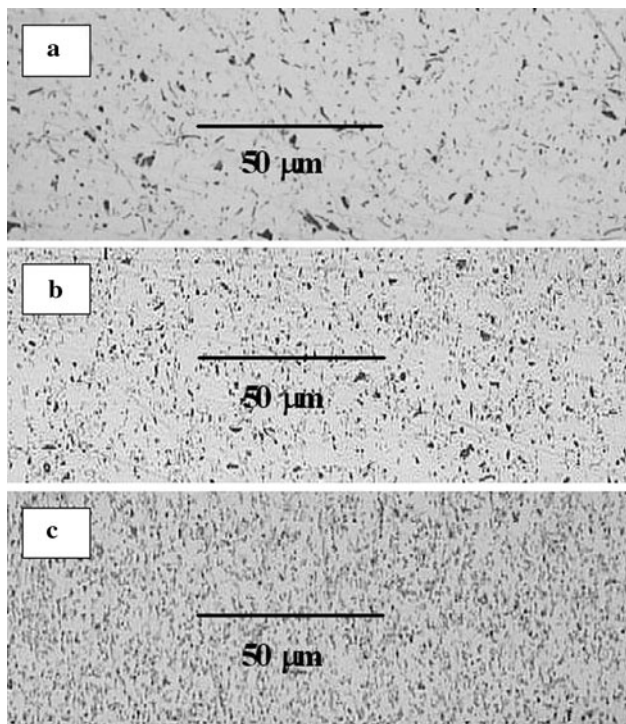


Fig. 1 Cross-sectional optical microscope images of electrodeposited **a** Ni–Al₂O₃-1, **b** Ni–Al₂O₃-2, and **c** Ni–Al₂O₃-3 coatings

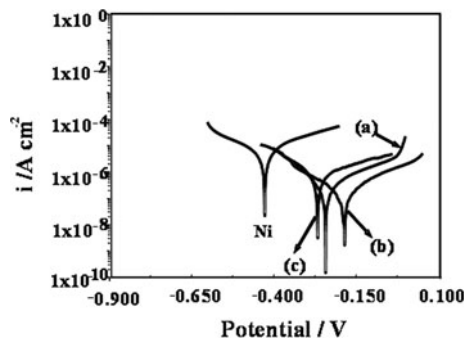


Fig. 2 Tafel plots of electrodeposited Ni (**a**) Ni–Al₂O₃-1, (**b**) Ni–Al₂O₃-2, and (**c**) Ni–Al₂O₃-3 coatings

very low indicating superior corrosion resistance of the coating. The R_p value of Ni–Al₂O₃-2 was the highest (131.5 kΩ cm²), implying better corrosion resistance of the coating compared to other coatings.

The Nyquist impedance plots and Bode plots for Ni and Ni–Al₂O₃ are, respectively, shown in Figs. 3, 4. From the Nyquist plot it is evident that the impedance offered by Ni–Al₂O₃-2 is higher than that of Ni–Al₂O₃-1, Ni–Al₂O₃-3, and pure Ni. In the Nyquist plot, the depressed semicircle with the center under the real axis is characteristic for the solid electrodes. At higher frequencies, interception with the real axis is ascribed to the electrolyte bulk resistance (R_s), and at low frequencies, an interphase appears whose interception with the real axis is ascribed to the charge transfer resistance (R_{ct}). In the Nyquist plot, the diameter of the semicircle corresponding to Ni and Ni–Al₂O₃ coatings increased compared to the substrate, thus indicating better corrosion resistance of the coatings. The shape of the impedance spectra describes the type of electrochemical reactions taking place on the electrode surface. The impedance plot of Ni shows single-time constant, and Ni–Al₂O₃ composites show the presence of two-time constant behavior. The higher-frequency time constant is related to the solution/coating interface, and lower-frequency time constant is related to the solution/substrate interface.

Bode plots of Ni and Ni–Al₂O₃ composite coatings are shown in Fig. 4. At frequencies below 10³ Hz, a capacitive response was obtained for Ni–Al₂O₃-2 (Fig. 4c). However, in other coatings the capacitance response is observed at 10⁴ Hz, and also narrow phase angle regions are observed. The Bode plot of Ni–Al₂O₃-2 shows a large negative shift in the Bode phase angle plot, and a straight line with a slope of about -1 in the Bode magnitude plot. These are the indications of higher corrosion resistance [24]. Coatings of Ni, Ni–Al₂O₃-1, and Ni–Al₂O₃-3 are less corrosion resistant than Ni–Al₂O₃-2, and they exhibit a low-frequency breakpoint just above 10 mHz. Coatings of Ni, Ni–Al₂O₃-1, and Ni–Al₂O₃-3 have much smaller capacitive regions across the frequency domain and distinct low frequency breakpoints which result in well-defined DC limits in the magnitude of the impedance. Ni–Al₂O₃-2 exhibits the highest DC limits. This type of EIS response shows improved corrosion resistance for Ni–Al₂O₃-2 compared with Ni, Ni–Al₂O₃-1 and Ni–Al₂O₃-3 [24].

The appropriate equivalent circuits used to fit the impedance spectra obtained for plain Ni and composite

Table 1 Corrosion potential, corrosion rates and Tafel slopes calculated from potentiodynamic diagrams for Ni–Al₂O₃-1, Ni–Al₂O₃-2, and Ni–Al₂O₃-3 compared with Ni

Sample details	i_{cor} (μA cm ⁻²)	E_{cor} (V)	R_p (kΩ cm ²)	bc (V dec ⁻¹)	ba (V dec ⁻¹)
Ni	0.6267	-0.451	4.82	0.115	0.139
Ni–Al ₂ O ₃ -1	0.0242	-0.242	92.98	0.093	0.119
Ni–Al ₂ O ₃ -2	0.0119	-0.184	131.5	0.098	0.100
Ni–Al ₂ O ₃ -3	0.0839	-0.267	42.2	0.128	0.236

Fig. 3 Nyquist plots of electrodeposited **a** Ni, **b** Ni-Al₂O₃-1, **c** Ni-Al₂O₃-2, and **d** Ni-Al₂O₃-3 coatings

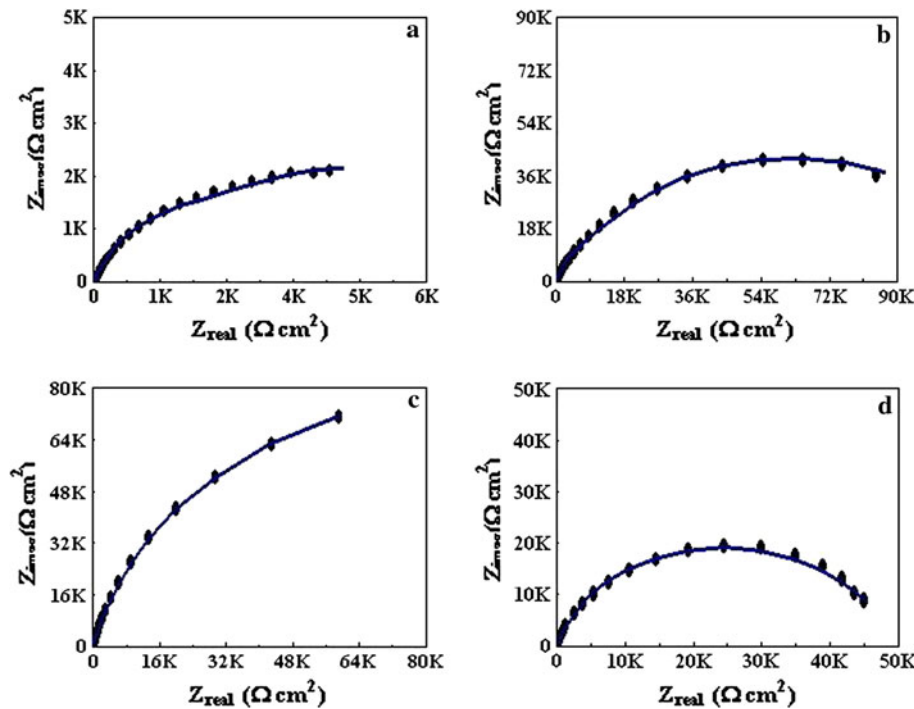
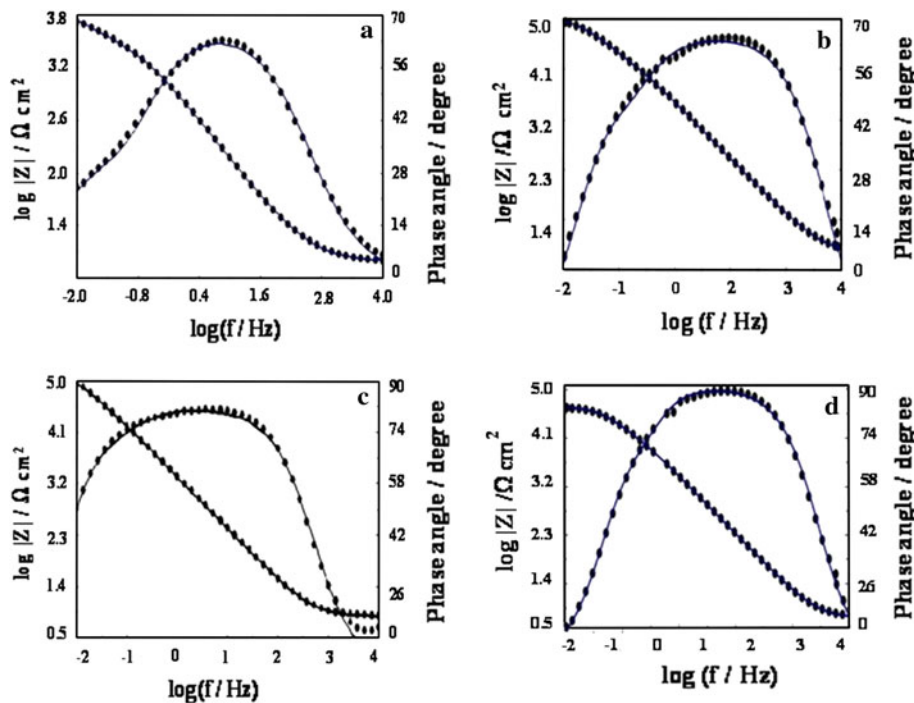


Fig. 4 Bode plots of electrodeposited **a** Ni, **b** Ni-Al₂O₃-1, **c** Ni-Al₂O₃-2, and **d** Ni-Al₂O₃-3 coatings



coatings are shown in the Fig. 5. The capacitance is replaced with constant phase element (CPE) for a better quality fit. CPE accounts for the deviation from ideal dielectric behavior and is related to the surface inhomogeneities. It must be noted that in the EQUIVCRT program, Q stands for constant phase element. The impedance

data obtained from the spectra are tabulated in Table 2. The R_{ct} value increases in the following order: Ni > Ni-Al₂O₃-3 > Ni-Al₂O₃-1 > Ni-Al₂O₃-2. Ni-Al₂O₃-2 which contains γ -Al₂O₃ shows higher R_{ct} value of about 164.5 k Ω cm², indicating better corrosion resistance compared to other coatings. The R_{coat} value obtained for

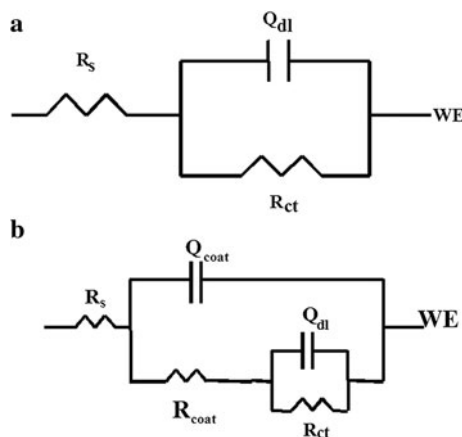


Fig. 5 Equivalent circuit for **a** Ni and **b** Ni-Al₂O₃ coatings (R_s solution resistance of test electrolyte between the working electrode and reference electrode, Q_{dl} double layer capacitance, R_{ct} charge transfer resistance, Q_{coat} coating capacitance, R_{coat} coating resistance, WE working electrode)

Ni-Al₂O₃-2 is the highest (155 kΩ cm²), which indicates that resistance offered by the coating is higher. Ni-Al₂O₃-1 containing α -Al₂O₃ shows very low Q_{coat} and Q_{dl} values of 35 and 4 μF cm⁻². The decrease in Y_0 of Q_{coat} and Q_{dl} may be due to the decrease in the area involved in the electrochemical reactions, i.e., a decrease in the surface area of the barrier coating in contact with the solution. The n_{dl} values for the nanocomposite coatings lie in between 0.82 and 0.87, indicating a deviation in the behavior of surface of the coatings from ideal capacitive behavior. From the potentiodynamic and impedance study, it can be concluded that the corrosion-resistant properties of the coatings decreased in the order: Ni-Al₂O₃-2 > Ni-Al₂O₃-1 > Ni-Al₂O₃-3 > Ni.

The SEM images of the surface of the samples after corrosion tests are shown in Fig. 6a, c, e and their respective EDAX spectra are shown in Fig. 6b, d, f. Surprisingly, there was a difference in the morphology of the Ni-composite coatings with a change in the crystallographic forms of the alumina particles. The SEM images clearly show the superior corrosion resistance of Ni-Al₂O₃-2 surface which has not reacted much to the corrosive media. On the other hand, the surfaces of Ni-Al₂O₃-1 and Ni-Al₂O₃-3 have reacted with the

corrosive media. The lowest corrosion resistance of Ni-Al₂O₃-3 is also evident from the appearance of Fe peak in the EDAX spectrum (Fig. 6f) which was absent in the EDAX spectra of other two samples. The lower corrosion resistance of Ni-Al₂O₃-3 may be due to the poor bonding between the particles and the matrix. There is a possibility of the dissolution of these loosely held alumina particles at high potentials; as a result, more nickel is exposed to the electrolyte for corrosion attack and hence poor corrosion resistance.

3.2 Wear studies

Wear results of Ni-Al₂O₃ composite coatings are tabulated in Table 3. It is evident from Table 3 that Ni-Al₂O₃-1 has lower wear volume and hence better wear resistance compared with Ni-Al₂O₃-2 and Ni-Al₂O₃-3 coatings according to Holm–Archard relationship [23, 24]. For Ni-Al₂O₃-1, the coefficient of friction was higher, which is probably due to the higher hardness of α -alumina phase present in the sample [23, 24]. The Ni-Al₂O₃-2 and Ni-Al₂O₃-3 coatings exhibited lower coefficient of friction values compared with Ni-Al₂O₃-1 probably because of the presence of gamma phase which is relatively softer compared with corundum α -phase. The optical micrographs obtained on the wear track and wear pin for Ni-Al₂O₃-1, Ni-Al₂O₃-2, and Ni-Al₂O₃-3 after wear tests are shown in Fig. 7.

The pin and disk corresponding to Ni-Al₂O₃-1 (Fig. 7a, b) show very less scouring marks, and the pin surface shows colored passive film. The pin surfaces corresponding to Ni-Al₂O₃-2 (Fig. 7c) and Ni-Al₂O₃-3 (Fig. 7e) do not show the passive film formation; instead, the disk and pins show more scouring marks compared with Ni-Al₂O₃-1. It is also evident that the Ni-Al₂O₃-1- and Ni-Al₂O₃-3-coated pins have undergone uniform wear, and the Ni-Al₂O₃-2-coated pin has undergone non-uniform wear. More material transfer from the pin to the disk is seen in Ni-Al₂O₃-2 (Fig. 7d) and Ni-Al₂O₃-3 (Fig. 7f).

The plots of sliding distance versus the wear loss for Ni-Al₂O₃ coatings are shown in Fig. 8. From the plots, it is evident that Ni-Al₂O₃-1 undergoes lower wear loss compared with Ni-Al₂O₃-2 and Ni-Al₂O₃-3. The plots of

Table 2 Electrochemical impedance analysis data

Sample details	R_s (Ω cm ²)	$Q_{coat}-Y_0$ (μF cm ⁻²)	n_{coat}	R_{coat} (kΩ cm ²)	$Q_{dl}-Y_0$ (μF cm ⁻²)	n_{dl}	R_{ct} (kΩ cm ²)
Ni	8.5	–	–	–	18.9	0.71	6.1
Ni-Al ₂ O ₃ -1	7.3	35.1	0.90	105.6	4.94	0.82	109.3
Ni-Al ₂ O ₃ -2	7.5	101.0	0.92	155.0	50.0	0.83	164.5
Ni-Al ₂ O ₃ -3	7.7	131	0.85	42.0	10.5	0.87	46.8

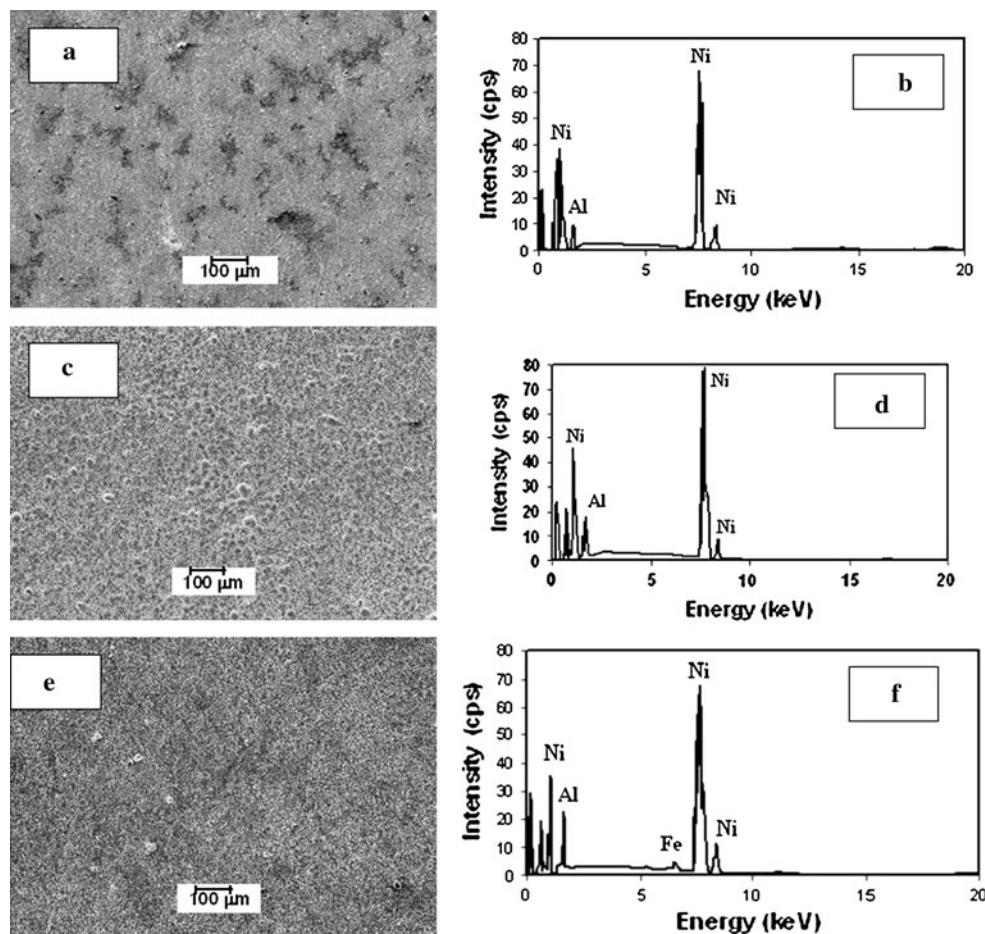


Fig. 6 SEM images of electrodeposited composite coatings after corrosion studies: **a** Ni–Al₂O₃-1, **c** Ni–Al₂O₃-2, and **e** Ni–Al₂O₃-3, and their corresponding EDAX spectra: **b** Ni–Al₂O₃-1, **d** Ni–Al₂O₃-2, and **f** Ni–Al₂O₃-3

Table 3 Wear result data of Ni–Al₂O₃ composite coatings

Sample	Total loss of height (μm)	Loss of height of pin (μm)	Coefficient of friction	Wear volume (mm ³)	Wear coefficient
Ni–Al ₂ O ₃ -1	22	21.22	0.819	0.0084	9.419×10^{-7}
Ni–Al ₂ O ₃ -2	42	41.7	0.760	0.0327	4.4097×10^{-6}
Ni–Al ₂ O ₃ -3	50	49.5	0.764	0.0799	7.478×10^{-6}

coefficient of friction versus sliding distance are shown in Fig. 9. From the plots it is evident that Ni–Al₂O₃-2 and Ni–Al₂O₃-3 exhibit similar coefficients of friction, which is lower than that of Ni–Al₂O₃-1.

The transfer of material from the pin to the disk was confirmed by the Raman spectra recorded on the wear track of disks (Fig. 10). The Raman spectrum of wear track of Ni–Al₂O₃-1 shows a peak around 650 cm⁻¹ which corresponds to Raman active phonon modes for corundum (α -Al₂O₃) as reported by Porto and Krishnan [25]. The Raman spectrum of wear track of Ni–Al₂O₃-2 shows peaks at 481, 558, and 680 cm⁻¹. The peaks at 481 and 680 cm⁻¹ correspond to gamma phase of alumina,

clearly indicating the transfer of material from the pin to the disk.

4 Conclusions

Different crystallographic forms of alumina particles like pure α -Al₂O₃ were prepared by solution combustion method, pure γ -Al₂O₃ was prepared by precipitation route, and commercial Alcoa alumina containing mixture of α and γ particles were codeposited with Ni at a current density 15.5 mA cm⁻² and 600 rpm magnetic stirrer speed. Ni–Al₂O₃-2 composite coating containing gamma-alumina

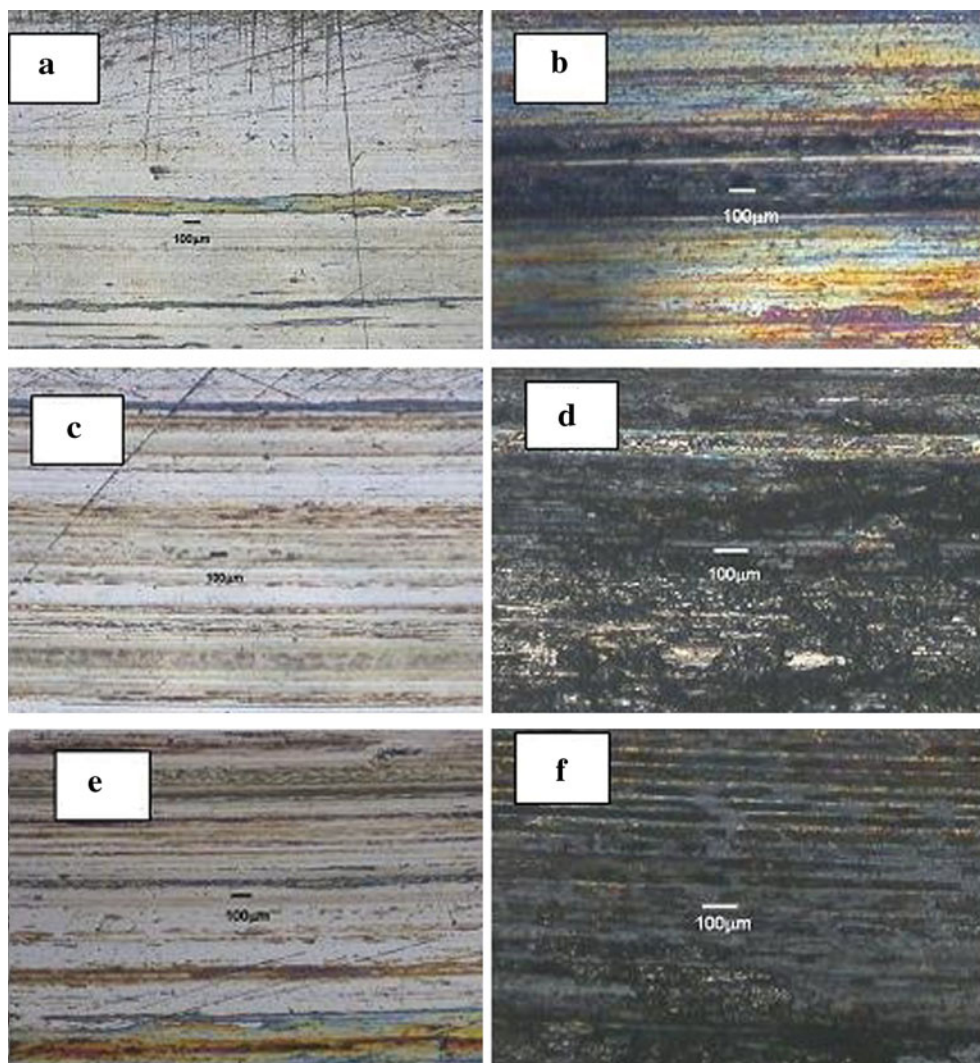


Fig. 7 Optical micrographs of the wear tracks of the pins coated with **a** Ni–Al₂O₃-1, **c** Ni–Al₂O₃-2, and **e** Ni–Al₂O₃-3 after wear tests; and **b**, **d**, and **f** are their corresponding wear tracks on discs

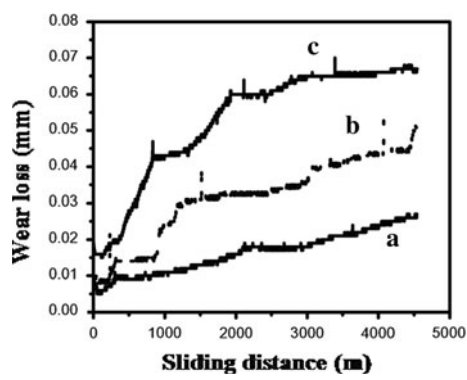


Fig. 8 Plots of wear loss versus the sliding distance measured using a pin-on-disk tribometer

phase showed an improved corrosion resistance relative to Ni–Al₂O₃-1 (containing alpha alumina) and Ni–Al₂O₃-3 (containing mixture of alumina phases). The wear resistance

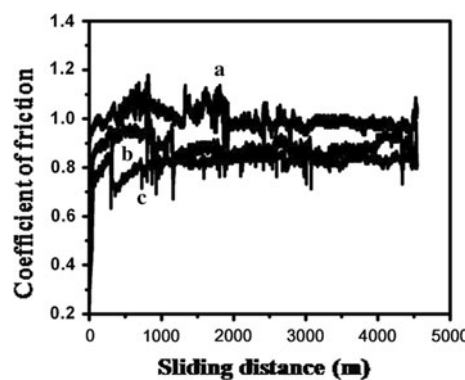


Fig. 9 Plots of coefficient of friction versus sliding distance measured using a pin-on-disk tribometer

of Ni–Al₂O₃-1 containing alpha alumina was higher than the Ni-composites containing gamma-alumina and mixture of alumina phases. Thus, it has been shown that the

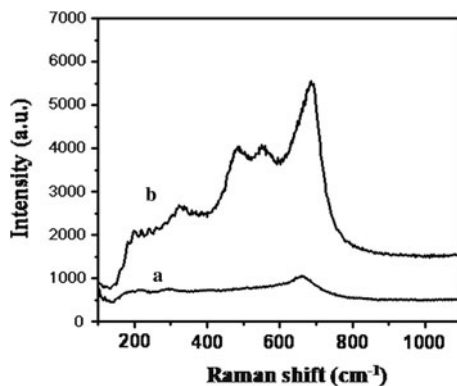


Fig. 10 Raman spectrum of wear track of (a) Ni-Al₂O₃-1 and (b) Ni-Al₂O₃-2 transferred disk

corrosion- and wear-resistant properties of nickel–alumina matrix vary with the phase of the incorporated alumina particles. Thus, by proper selection of pure phases of alpha- and gamma-alumina phases, it may be possible to get the preferred properties.

Acknowledgments The authors acknowledge Director, NAL for his constant encouragement. The authors thank Mr. Muniprakash for carrying out the wear studies, and Ms. Divya and Mr. N. Balaji for the preparation of powders and composites. The authors thank Mr. Raghavendra for the SEM measurements, and Mr. Manikandanath for the Raman studies.

References

- Bonino J-P, Loubiere S, Rousset A (1998) J Appl Electrochem 28:1227
- Feng Q, Li T, Yue H, Qi K, Bai F, Jin J (2008) Appl Surf Sci 254:2262
- Dong YS, Lin PH, Wang HX (2006) Surf Coat Technol 200:3633
- Banovic SW, Barmak K, Marder AR (1999) J Mater Sci 34:3203
- Du L, Xu B, Dong S, Yang H, Wu W (2005) Surf Coat Technol 192:311
- Jakob C, Romanus H, Spiess L, Wielage B, Lampke T, Steinhäuser S (2003) Electrochim Acta 48:3063
- Bund A, Thiemig D (2007) Surf Coat Technol 201:7092
- Fawzy MH, Ashour MM, Abd El-Halim AM (1996) Trans Inst Metal Finish 74(2):72
- Shao I, Verecken PM, Cammarate RC, Seaton PC (2002) J Electrochem Soc 149:C610
- Neckarsulm NSU (1970) Br Patent 1200:410
- Roos JR, Celis JP, Kelchtermans H (1978) Thin Solid Films 54:173
- Sautter FK (1963) J Electrochem Soc 110:557
- Karayannidis HS, Batis G, Vassiliou P (1999) Anti-Corros Meth Mater 46:29
- Szczygiel B, Kolodziej M (2005) Electrochim Acta 50:4188
- Ciubotariu A-C, Benea L, Magda L-V, Dragan V (2008) Electrochim Acta 53:4557
- Szczygie B, Koodziej (2005) Trans Inst Metal Finish 83(4):181
- Wang S-C, Wei W-CJ (2003) J Mater Res 18(7):1566
- Feng Q, Li T, Zhang Z, Zhang J, Liu M, Jin J (2007) Surf Coat Technol 201:6247
- Aruna ST, William Grips VK, Rajam KS (2010) J Appl Electrochem 40:2161
- Aruna ST, Bindu CN, Ezhil Selvi V, William Grips VK, Rajam KS (2006) Surf Coat Technol 200:6871
- Aruna ST, William Grips VK, Ezhil Selvi V, Rajam KS (2007) J Appl Electrochem 37:991
- Holm R (1946) Electric contacts, Sect. 40. Almquist and Wiksell, Stockholm
- Archard JF (1953) J Appl Phys 24:981
- Kelly RG, Scully JR, Shoesmith DW, Buchheit RG (2003) Electrochemical techniques in corrosion science and engineering, Chap. 8. Marcel-Dekker, New York, pp 296–298
- Porto SPS, Krishnan RS (1967) J Chem Phys 47:1009